Journal of Power Sources 438 (2019) 226971

Contents lists available at ScienceDirect

Journal of Power Sources

journal homepage: www.elsevier.com/locate/jpowsour

Prediction of the heavy charging current effect on nickel-rich/silicon-graphite power batteries based on adiabatic rate calorimetry measurement

Hang Li, Chaoyue Liu, Xiangbang Kong, Jun Cheng [**], Jinbao Zhao [*]

State Key Lab of Physical Chemistry of Solid Surfaces, Collaborative Innovation Centre of Chemistry for Energy Materials, State-Province Joint Engineering Laboratory of Power Source Technology for New Energy Vehicle, Engineering Research Center of Electrochemical Technology, Ministry of Education, College of Chemistry and Chemical Engineering, Xiamen University, Xiamen, 361005, PR China

HIGHLIGHTS

- The electrochemical-thermal model of power lithium ion battery is made.
- The new solution for the prevention of thermal runaway is proposed.
- The relationship of ambient temperature and maximum safe charge current is found.
- The design parameters of battery will affect the relationship.
- The result will guide the design of battery and battery thermal management system.

ARTICLE INFO

Keywords:
Large capacity
Power lithium ion battery
Heavy current charge
Thermal runaway prevention
Lithium ion battery optimization design

ABSTRACT

The $LiNi_{0.8}Mn_{0.1}Co_{0.1}O_2$/Silicon-carbon (NCM811/Si@C) lithium ion battery is used in the plug-in electric vehicle due to its high specific energy. The mileage of electric vehicles can be improved by increasing the energy density of batteries, but the charging process becomes a more challenge issue since the excessive charging current results in high temperature while the thermal stability of NCM811 material is poor. Also, the increasing of temperature may cause the thermal runaway of lithium ion battery. In this work, in order to study the thermal runaway prevention during charging process, the NCM811/Si@C battery model is set up, and the simulation results are verified by the experimental results. The detailed temperature distribution of the battery is observed, which can advise on the thermal management system of the batteries. Based on the thermal runaway data, the maximum safe charge current under different ambient temperature is predicted, and the relationship between maximum safe charging current and ambient temperature is found.

1. Introduction

As the global energy crisis continues to intensify and the environmental changes caused by the long-term use of fossil fuels become more and more serious, the use of clear energy sources to replace the original fossil fuels, such as oil and coal, has become an inevitable trend to improve of the global environment [1–5]. The lithium ion batteries are being used on a large scale because of their high capacity, long cycle life, low carbon and no memory effect [6,7]. Due to the development of society, the lithium ion batteries have already been used in electric vehicles (EV), mobile phones, and computers. As a consequence, the batteries with higher energy density become urgent demanding. Thus, the Lithium ion batteries with high energy capacity have become the research focus recently [8–10].

However, the range anxiety has become the largest obstacle for the wide usage of electric vehicles [11]. According to the US National Benchmark Report (2016), over half (54%) of US consumers consider to purchase an EV when the range of the car at least 175 miles [12]. The

* Corresponding author.
** Corresponding author.
E-mail address: jbzhao@xmu.edu.cn (J. Zhao).

https://doi.org/10.1016/j.jpowsour.2019.226971
Received 17 June 2019; Received in revised form 17 July 2019; Accepted 2 August 2019
Available online 6 August 2019
0378-7753/© 2019 Elsevier B.V. All rights reserved.

expected value of the energy density of lithium ion batteries in the "Made in China 2025" program is 300 W kg^{-1} [13]. As we can see, the capacity of Li-ion battery majorly depends on cathode materials. Comparing with the classical cathode material $LiCoO_2$, the $LiNi_xCo_yMn_zO2$ (x + y + z = 1, also known as NCM) has higher achievable specific capacity and operating voltage. Moreover, the cost of this material is lower because the Co content is reduced [5]. Shabbir et al. [14] used the spreadsheet tool BatPaC to calculate the pack level energy density, specific energy and battery cost. And the cathode materials which they calculated include the $LiNi_{0.3}Co_{0.3}Mn_{0.3}O_2$ (NCM333, also known as NCM111), $LiNi_{0.5}Co_{0.2}Mn_{0.3}O_2$ (NCM523), $LiNi_{0.6}Co_{0.2}Mn_{0.2}O_2$ (NCM622), $LiNi_{0.4}Co_{0.3}Mn_{0.3}O_2$ (NCM433), $LiNi_{0.8}Co_{0.1}Mn_{0.1}O_2$ (NCM811), and $LiNi_{0.4}Co_{0.4}Mn_{0.2}O_2$ (NCM422). The result shows that specific capacity of NCM811 is the largest at high upper cutoff voltages (UCV). Moreover, the NCM811 offers the lowest cost at high UCV in all of NCM materials [14]. In order to achieve the goal of "Made in China 2025", the most valuable cathode materials are ternary oxide cathodes, especially NCM811.

To match NCM cathode material, the anode material should be the graphite with silicon added [15]. The theoretical specific capacity of silicon could reach to 4000 mAh·g^{-1} [16,17]. However, the volume change of Si during lithiation/delithiation process is very huge (almost 400%). The volume change can bring some serious problems such as capacity fade, internal short, and so on [17–21]. The silicon oxide is considered as a suitable substitute for silicon due to small volume change during the charge/discharge process [22]. Although silicon oxide has so many advantages, the usage is still limited because of its low conductivity and low coulombic efficiency [23–25]. To solve this problem, the silicon-based anode materials used in commercial production usually are always blended with graphite.

Though the NCM811/Si@C Li-ion batteries have higher capacity, the Ni-rich NCM cathodes usually show poor thermal stabilities [26], which may lead to severe potential safety problems, such as thermal runaway [27–29]. The thermal runaway reaction of the battery is a series of reactions of the materials inside the lithium ion battery. When the critical temperature is reached, some irreversible and intense exothermic reactions occur inside the batteries [15,29–31]. These reactions cause the battery temperature to rise sharply, causing the battery to fail or even explode. The reasons for the thermal runaway of the battery are mainly about mechanical abuse, charge abuse, and heat abuse [29].

Besides the range anxiety, another major anxiety for electric car users is the charging. Users want the battery to store more energy and hope to be fully charged in a shorter time. Limiting the speed of battery charging, in addition to the impact of the utility industry, the critical issue is that the battery is likely to cause safety problems in a fast charging state. Yan et al. [32] have reported that when the battery is charged at 10 C, the battery temperature change can be equivalent to the thermal runaway. According to the usage habits of the battery, compared with the discharge process, the battery is not always taken care of during the charging process. If the battery charging temperature is not well managed, it will lead to serious consequences. The thermal runaway occurred during the charge process will be more destructive than discharge process. Being able to predict the maximum safe charging current of the battery is a good way to avoid the thermal runaway.

This work uses the COMSOL Multiphysics software to simulate the temperature change of the 57 Ah pouch NCM811/Si@C lithium ion battery at different charge rates and compares it to the actual measured temperature. At the same time, according to the battery thermal runaway data measured by Adiabatic Rate Calorimetry (ARC), the safety during battery charging is predicted, and the maximum safe charging current at different ambient temperatures is predicted. Besides, based on the sweep data of different ratio battery, the function of maximum safe charge current and the ambient is founded.

Table 1
The geometry parameters of lithium ion battery.

Capacity (Ah)	Work Voltage (V)	Length (mm)	Width (mm)	Thickness (mm)
57	2.8–4.2	264	92	12

2. Model and validation

2.1. Model

This model mainly includes two parts, electrochemical and heat transfer, which are interrelated with temperature. The electrochemical model we used is the pseudo two-dimensional (P2D) model based on the study by Newman and Doyle [33–35]. The lithium ion battery has five parts: anode, cathode, electrolyte, separator, and current collector. The electrochemical model includes five processes as followed:

(i) Electron conduction in the current collector. This process is based on the *Ohm*'s law.
(ii) Ionic transport in the electrodes, electrolyte and separator. This process is based on the *Nernst-Planck* equation.
(iii) Chemical reaction in the surface of material. This reaction is based on the *Butler-Volmer* electrode kinetics equation.
(iv) Ionic transport in the material. This process is based on the *Fick*'s second law.
(v) Ionic conduction in the electrodes, electrolyte. This process allows the *Ohm*'s law, allowing for the introduction of the effect of activity and electromigration.

The heat transfer model mainly consists of three parts:

(i) Reversible heat because of entropy change during charge and discharge processes.
(ii) Irreversible heat due to the electrochemical reaction polarization between electrode and the electrolyte.
(iii) Ohmic heat owing to present of the Ohmic resistance.

All of the equations involved have been built in COMSOL Multiphysics. It is only necessary to establish the corresponding model and input specific parameters when performing the simulation. The simulation model size is exactly the same as the real battery size. The lithium ion battery simulated contains a total of 31 pieces of cathode electrode and 32 pieces of anode electrode. The pouch lithium ion battery made by JEVE. The battery we used is an experimental model. The 57 Ah is the design capacity, the discharge capacity we measured was about 55 Ah. The battery size is as described in the Table 1:

The lithium ion battery model shows in Fig. 1. The left model is a 1:1 model built with reference to the actual lithium ion battery, and the middle is a detailed view of the y-axis magnified 50 times, the right model is a single cell.

The battery cathode and anode current collector are distributed at both ends of the battery, the anode current collector at the bottom of battery and the cathode current collector at the top of battery in the model, as shown in Fig. 1. In order to release more energy of the cathode electrode materials, the battery is designed to make anode electrode wrap the cathode electrode. Besides, the cathode and anode electrode are double-coated active materials.

2.2. Boundary condition

The electrochemical-thermal model simulates the voltage and temperature changes of lithium ion battery during charging process, and needs to solve the corresponding mass transfer and heat transfer equation. The equations have been reported in some literatures [7,32,36–39], so here will not explain. These equations are all the partial

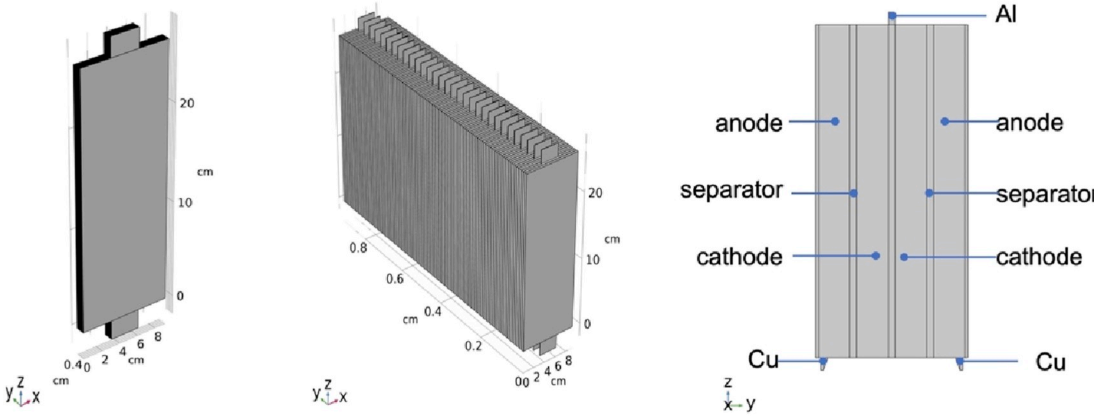

Fig. 1. The model of lithium ion battery.

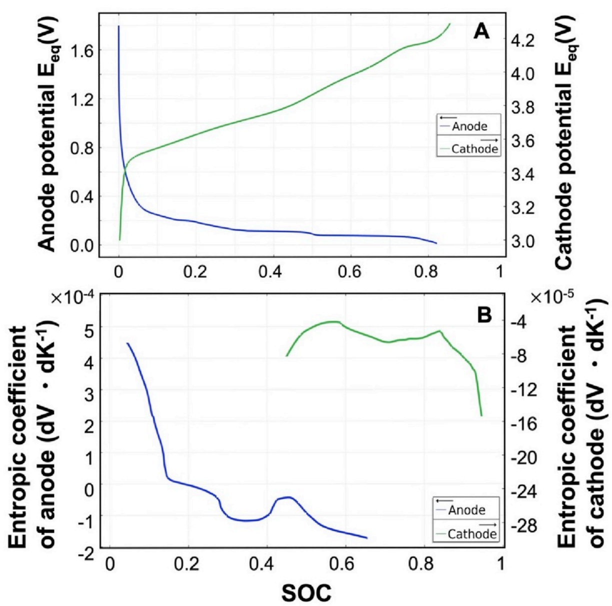

Fig. 2. The equilibrium potential and the entropic coefficient of anode and cathode used in the model.

differential equations(PDE), to solve those PDEs, the model should set corresponding boundary condition.

In the lithium ion battery module, the cathode tabs are set the charge current boundary condition, but the anode tabs are set to the grounding boundary condition, which means that the potential of anode tabs is 0 V. The charge stop condition is set the voltage of lithium ion battery research to 4.2 V. Besides, the temperature used in lithium ion battery module is the temperature calculated by solid heat transfer module.

In the solid heat transfer module, the heat source of electrochemical reaction thermal is set on the lithium ion battery. The electrochemical reaction heat which has mentioned above is calculated by the multi-physics coupling. The boundary condition of the battery surface is natural air convection heat transfer, and the ambient temperature is set to the temperature same as the isothermal condition.

2.3. Parameters

This work is based on a three-dimensional lithium ion battery model. In order to accurately simulate the charging temperature change of the lithium ion battery, precise parameters need to be entered in the software. In this work, most of the parameters of the battery was measured. For parts of parameters, we refer to the parameters in the relevant literature. The specific parameters are put in the file of supporting information.

2.4. Equilibrium potential

To get the equilibrium potential, a button battery has been made for the research. After disassembling the fresh lithium ion battery, drying the electrode in an oven, followed by scraping the side of the double-coated electrode material pole piece with a scalpel, and re-cutting the piece of electrode, then a CR2016 type lithium ion battery has been made. Using lithium metal for the counter electrode, the current at 0.02 C charging is performed to obtain the equilibrium potential of the cathode and anode materials. The equilibrium potential is shown in Fig. 2A. When the cathode electrode material is discharged at about 3 V, the voltage drops sharply. Hence, the potential of cathode material equals 3 V is defined the state of charge (SOC) to 0. In this method, it is defined that the potential of anode material equals to 1.8 V as the SOC equals to 0.

The entropic coefficient represents the electrochemical heat released when the electrode material reacts under different SOC. The entropic coefficient used in this model is an Interpolation function as show in Fig .2B. For the SOC not marked in the figure, the entropic coefficient is taken by linear extrapolation.

2.5. Temperature and voltage file

The electrochemical-thermal coupling model of a battery requires coupling calculations of two physics fields, hence, it is necessary to verify both the voltage and temperature change of the battery during charge process. The battery voltage data are obtained from the Neware 5V100A Battery Test System (China). The charge and discharge step is a constant current discharge of the battery to 2.8 V, followed by constant current (30 A, 42 A, 57 A) charging to 4.2 V. The battery charging process temperature data are obtained from a HEL PHITEC BTC 500 (British) calorimeter with a constant ambient temperature of 20 °C. In the test, two thermocouples are placed on the center surface of the battery to capture the average temperature change of the battery.

The battery thermal runaway experiment is measured using the HEL PHITEC BTC 500 (British). The battery is charged to 4.2 V with constant current and constant voltage (CCCV) before being placed inside the ARC. When conducting the experiment, it is set that the initial calibration temperature is 25 °C, and the initial calibration time is 2 h. The heating rate is 5 °C $\cdot$min^{-1} in heat-up process and the search time is 10 min in search process. If the battery heat release rate is detected to be greater than 0.02 °C $\cdot$min^{-1}, the ARC will enter the adiabatic-track process. Before the ARC test, the heater is wound around the surface of the battery, and a thermocouple is attached to the center surface of the

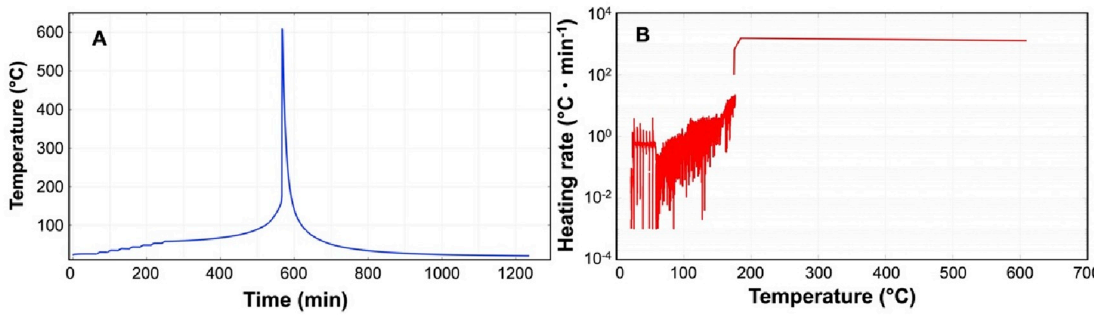

Fig. 3. Thermal runaway data of the NCM811/Si@C lithium ion battery.

battery to get the temperature of thermal runaway, and then the battery is wrapped with an aluminum tape.

3. Results and discussion

3.1. Thermal runaway data

The battery thermal runaway experiment is carried out before the simulation. The thermal runaway temperature and heating rate of the battery are shown in Fig. 3. It can be seen that the battery will enter the self-heating process at around 59.5 °C. This process indicates that the battery will enter dangerous state if the battery works over this temperature. This temperature (59.5 °C) is the threshold for normal use of the battery. When the battery temperature reaches 150 °C, the battery temperature will go out of control, and the battery will undergo a violent thermal runaway reaction. This temperature (150 °C) is the threshold for safe use of the battery. The heating rate can reach to 10^3 °C·min^{-1} when the thermal runaway occurs. According to the data of the adiabatic temperature rise of the battery, it can be concluded that the safe temperature of the battery is 150 °C, but the temperature for normal use should be lower than 59.5 °C. There are many reports that the first occurrence of an exothermic reaction in the thermal runaway reaction of a battery is the decomposition of the solid electrolyte interface (SEI) [9,29,40]. The SEI of the battery has an effect on the capacity,

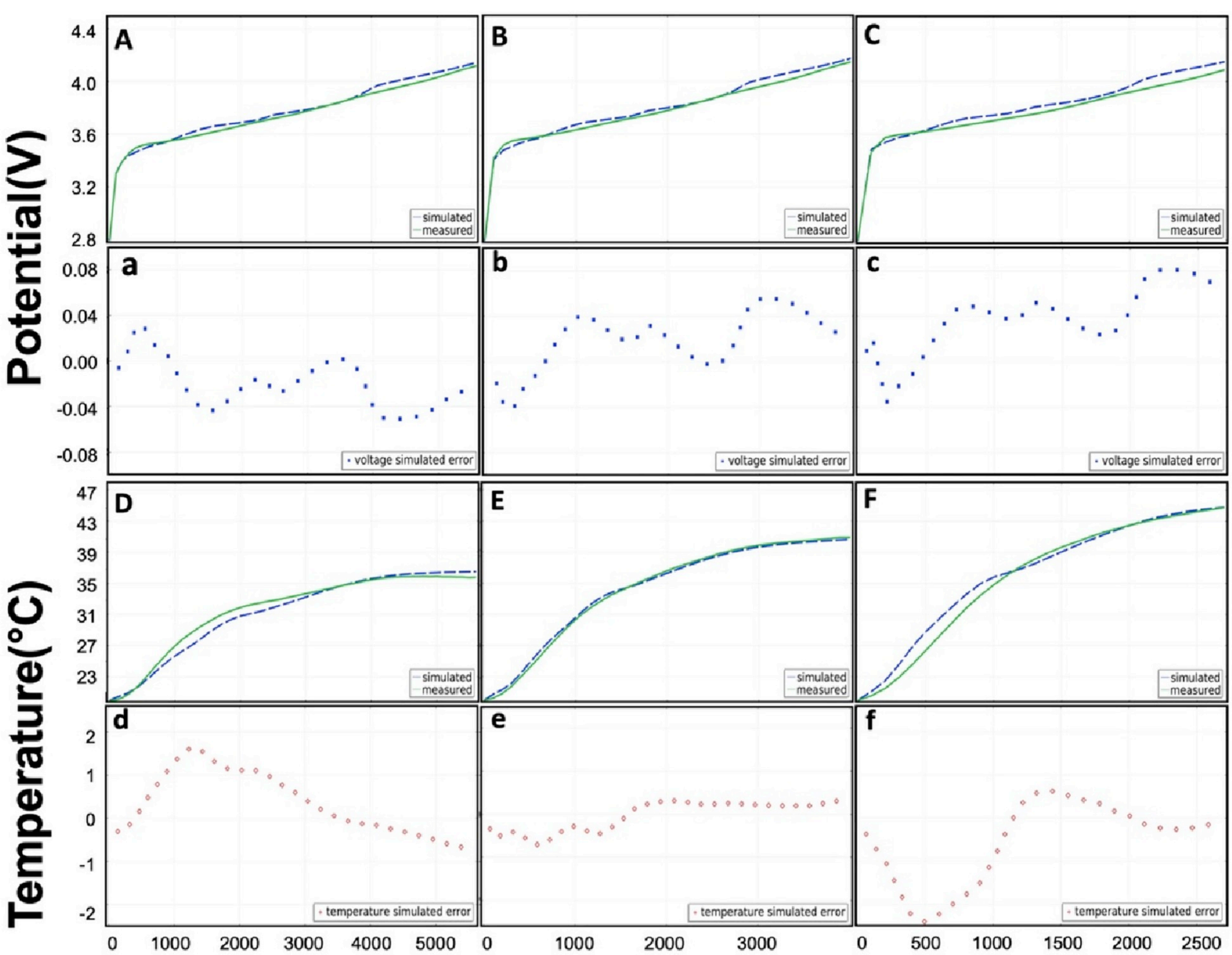

Fig. 4. The charge voltage and temperature simulation result. The A(D), B(E), and C(F), are the charge current equal to 30 A(~0.5C), 42 A(~0.7C), 57 A(1C), and the a, b, and c are the voltage simulation error respectively, the d, e, f are the temperature simulation error respectively.

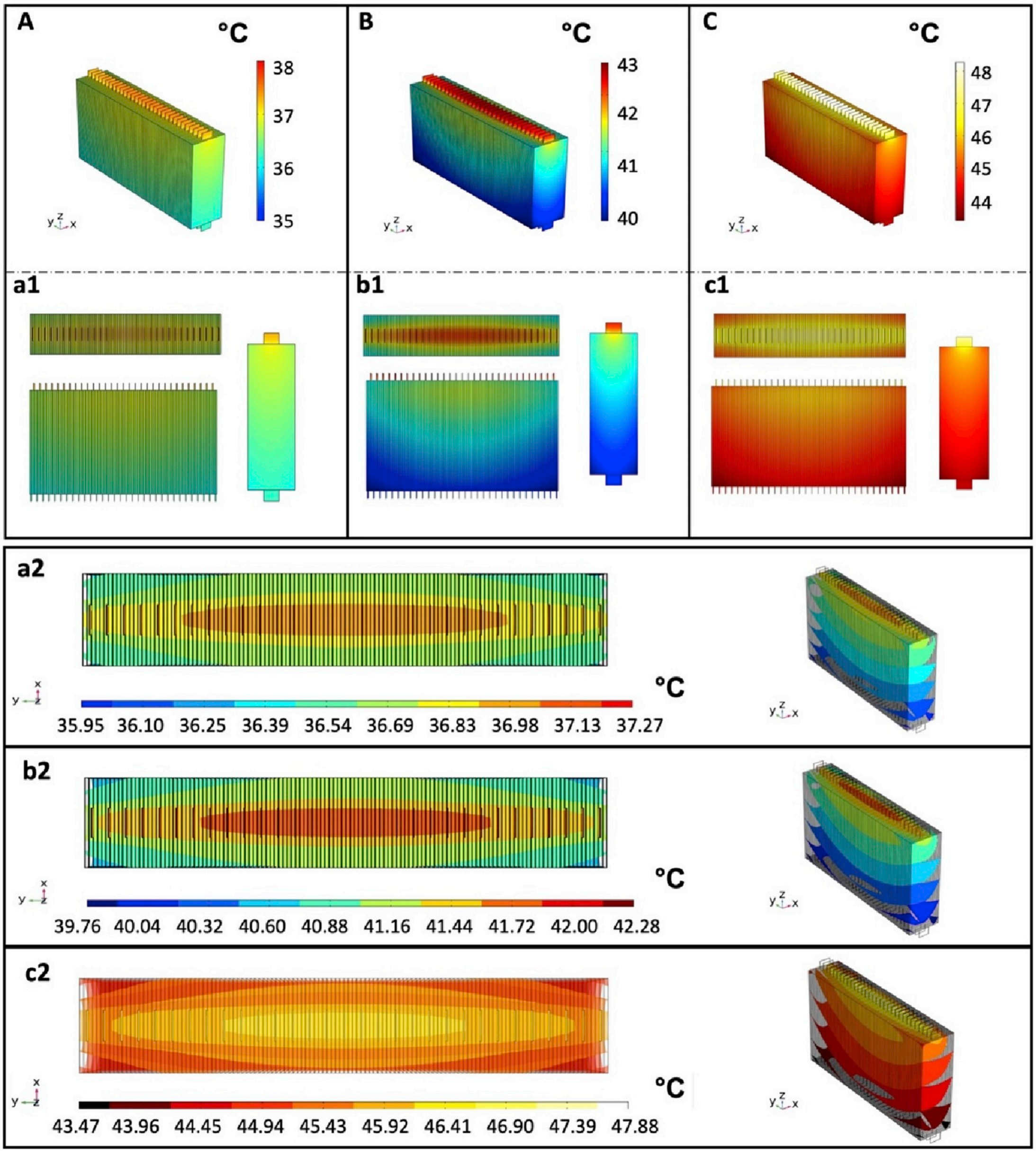

Fig. 5. The A (a1), B (b1), and C (c1) are the temperature distribution at the end of charging for 30 A, 42 A, and 57 A, respectively. The a2, b2, c2 are the top view of temperature distribution and the temperature gradient diagrams.

charge-discharge rate, safety and so on [41], hence, the SEI is very important for lithium ion battery. The ARC result is very helpful in determining whether the battery is in a safe state. In order to better use the lithium ion battery and make safe, the operate temperature of lithium ion battery should be lower than 59.5 °C. The 59.5 °C is defined as the reference temperature to find the maximum safe charging current during charging.

3.2. Lithium ion battery charge simulation

The 3D model is made and simulated in the COMSOL. This part of work is to calibrate the model in the early stages. The measurement data have been obtained at an ambient temperature of 20 °C, hence, the environment temperature of simulation is set to 20 °C.

The model validation considers changes in the electrochemical properties of the battery as well as changes in thermodynamics (temperature). The battery has been tested for the charge current of 57 A (1 C), 42 A (~0.7 C), and 30 A (~0.5 C) current, respectively. The temperature measured is the average temperature at the center of battery, and the temperature simulated is also the average temperature at the center of battery. The temperature of lithium ion battery at the end of charge is 36.2 °C, 41.5 °C, 45.7 °C under the current of 30 A, 42 A, 57 A in Fig .4. It is obvious that the temperature at the end of charge is increased with the charge current increase.

In order to evaluate the accuracy of the model, the error value is introduced, and the value of error equals to the value measured minus the value simulated. It can be found that the error of voltage and temperature between the simulation and the measurement result is within a stable range as shown in Fig. 4. The maximum voltage error between the simulation and measurement is 0.08 V in Fig. 4c, and the maximum error between the temperature simulation and the actual measurement is 2.5 °C in Fig. 4f. It can be considered that the simulation has a good consistency with the actual situation. In different charging current tests, the voltage simulation and temperature simulation under 30 A and 42 A charging currents are relatively more accurate. In the case of 57 A charging current, the temperature of the battery in the early stage of

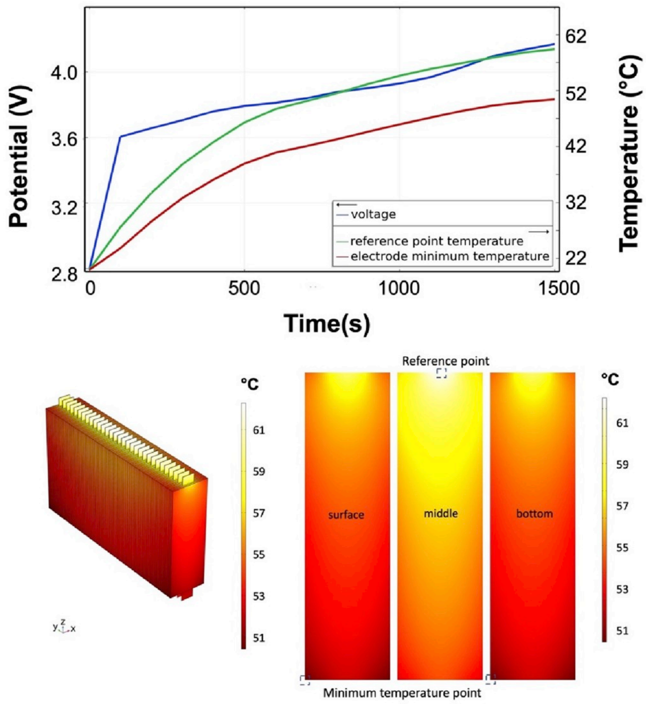

Fig. 6. The voltage and temperature change under maximum safe charge current at 20 °C ambient temperature.

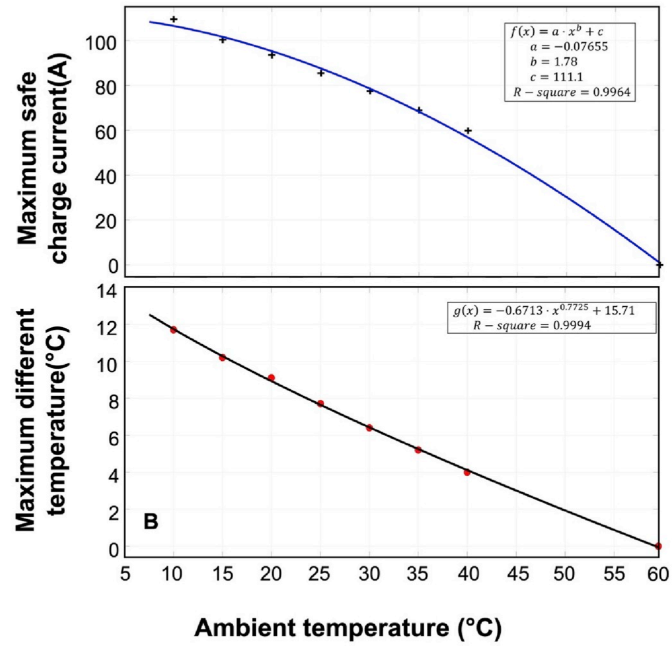

Fig. 7. The maximum safe charge current and the maximum different temperature have a power relationship with the ambient temperature.

charging has a relatively large error compared with the actual temperature, but in other cases, the simulation is consistent with the actual situation generally.

The distribution of the battery temperature at the end of charging of the battery is shown in Fig. 5. According to the simulation results, it can be seen that the temperature of cathode region is at its maximum, and this simulation conclusion is also the same as the actual battery charging process. There are two following reasons for this characteristic. First, since the conductivity of the cathode electrode material is lower than that of the anode electrode material, so the polarization heat in the cathode electrode portion is more than that in the anode electrode part. Second, the thermal conductivity of the cathode electrode material is lower than that of the anode electrode material, and the generated heat is difficult to diffuse quickly, causing a cumulative increase in temperature. When the battery is charged under different charging currents, the temperature difference of the battery at the end of charging, namely the electrode maximum temperature minus electrode minimum temperature, increases as the charging current increases. The temperature difference at 30 A charge current is 1.42 °C, the temperature difference at 42 A charge current is 2.52 °C, and the temperature difference at 57 A charge current is 4.41 °C.

The detail of temperature distribution of the battery at the end of charging can be got from the top view in Fig. 5 (a2, b2, c2), and it can be found that the temperature in the central of the cathode electrode near the tab is the largest. This can also be observed from the temperature gradient of the battery in Fig. 5, while the lowest temperature of the battery is near the edge of the anode tab of the battery. The temperature distribution of the battery appears to be circularly diffused from the cathode electrode tab of the battery to the anode electrode tab, which can be seen from the temperature gradient diagram of the battery in Fig. 5.

3.3. Maximum safe charge current simulation

According to the above simulation result, it can be found that the maximum temperature point at the end of the battery charging is at the junction of the 14th cathode electrode and the tab. Therefore, this point temperature is taken as the reference point to get the maximum safe charge current.

At an ambient temperature of 20 °C, we have used a parametric sweep to find the maximum safe current which the reference point reaches the reference temperature at the end of charging. The calculation results show that when the charging current is 1.64C (93.48 A), the reference point reaches the temperature of 59.5 °C at the end of charging, and the charging process voltage and the reference point temperature change as shown in Fig. 6. By comparing the temperature of the reference point with the average temperature of the surface of battery, as the charging time is extended, the difference between the two temperatures is continuously increased. This confirms that using the temperature of reference point as the benchmark for the simulation is correct.

Comparing the battery temperature at ambient 20 °C with the temperature profile at the end of 1.64 C charging, it can be found that the cathode electrode surface at the center of battery reaches the reference temperature, but the corresponding tab temperature has exceeded the reference temperature. It can be inference that the temperature change of the battery during charging is mainly caused by the ohmic heat generated by the battery current collector. At the same time, it is observed that the temperature of the two surfaces of battery in the y direction is consistent, which can be easily seen in the temperature profile.

Taking into account the ambient temperature changes during the use of battery, taking the annual temperature in Xiamen as an example, we have simulated the maximum safe current which the reference point reaches the reference temperature, and the maximum safe current can be used when the battery was charged at an ambient temperature of 10 °C–40 °C. The temperature gradient is 5 °C. The calculation results

Table 2
The geometric parameters of lithium ion battery scanned.

Length(mm)	528	264	198	132	44	33
Width(mm)	46	92	122.7	184	552	736
Ratio	11.48	2.87	1.61	0.72	0.08	0.05

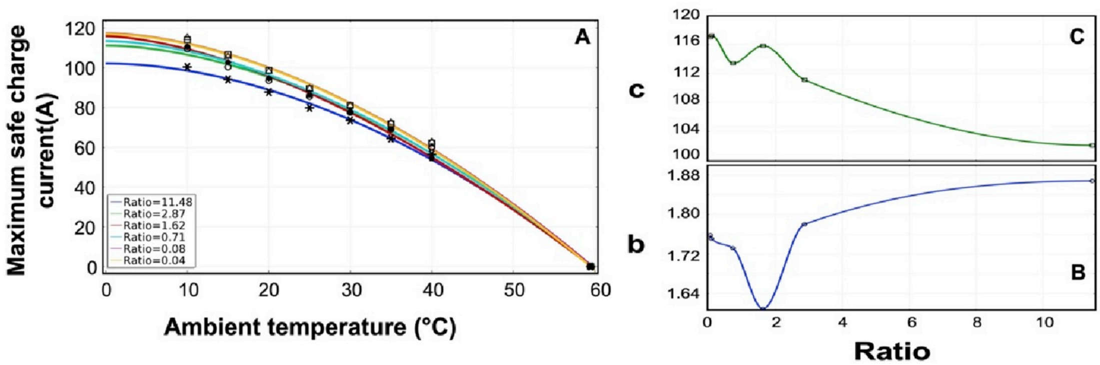

Fig. 8. Parameter scan result. The A is the fitting function in different ratios, the B and C are the coefficient b and c of the function.

are shown in the Fig. 7.

The charging current of the battery at different ambient temperatures gradually decreases with the increase of the ambient temperature. In addition, the difference between the minimum temperature and the maximum temperature, namely the maximum temperature difference, of the surface of battery electrode also gradually decreases. Using a function to fit these values, it can be seen that the maximum safe charging current has a power relationship with the ambient temperature. The function is as following:

$$f(x) = a \cdot x^b + c \tag{1}$$

where the x presents the ambient temperature, a is -0.07655, b is 1.78, and c is 111.1. The coefficient a is an adjustment factor. The coefficient b determines the shape of the function, it determines the extent to which the battery is affected by ambient temperature. The coefficient c indicates the maximum safe charging current. The temperature difference of battery also has a power relationship with the ambient temperature. The function is as following:

$$g(x) = -0.6714 \cdot x^{0.7725} + 15.71 \tag{2}$$

By analyzing these equations, it can be found that the maximum safe charge current will approach a stable value in a low ambient temperature as shown in Fig. 7. The reason can be considered that when the battery is in a low ambient temperature, the chemical reaction rate of the battery is relatively low, and the electrochemical heat generation is relatively small, but the ohmic heat generated by the current collector occupies a major portion, hence the heat mainly accumulates in the current collector. However, in a higher ambient temperature, the maximum safe charge current will decrease sharply, and the reason can be attached to that the chemical reaction is accelerated due to the ambient temperature increase. Therefore, from the point mentioned above, these two equations can be considered to be correct. From the function (1), the battery has a maximum safe charging current of 111.1 A. However, the lithium deposit and other side reactions will occur as the lithium ion battery in a low ambient temperature, and this electrochemical-thermal model doesn't consider this problem, hence there should be more consideration in low ambient temperature. Importantly, it is effective to use these two equations for the maximum safe charge current prediction of the battery at normal temperature.

Based on this method, the relationship between the ratio of the battery length/width and the maximum charging current is desired to be found. The different ratio in Table 2 has been scanned in this simulation, and the volume and the capacity of the battery has been controlled at a fixed value.

In function (1), when the value of b decreases, it means that the difference between the maximum charging currents of the battery at different ambient temperatures increases. When the value of b increases, it means that the battery has a larger charging current in same ambient temperature. From the results scanned, it can be found that the b value decreases first and then increases as the ratio increases. When the ratio equals to 1.61, the b gets the local minimum, which indicates that the maximum charging current of the battery is slightly affected by the ambient temperature. When value b gets to the local minimum means that the maximum safe charge current will be larger in the same ambient temperature. Based on the results in Fig. 8, to reduce the impact of battery geometry on maximum charging current, the ratio of the battery should be controlled to close to 1.61.

According to the temperature distribution above, it can be considered that the battery thermal management system (BTMS) should pay more attention to the cooling of the cathode electrode area of the battery during the charge process in order to avoid thermal runaway caused by local overheating. The use of different regions for different cooling powers enables the BTMS to be more efficient and the battery efficiency to be improved. The BTMS also needs a power to drive, and this method can save energy of cooling the battery while preventing thermal runaway. In addition, in order to make the temperature more uniform during charging, the ratio of the battery length/width should be reasonably controlled. Using the methods of simulating and parametric scanning, the design of battery geometry will be more reliable.

4. Conclusion

This work has made the NCM811/Si@C lithium ion battery model, and verified it at different charge rates to prove that the model is correct and effective. It is found that the maximum temperature point is at the middle of cathode, but the minimum temperature point is at the edge of anode. The battery thermal runaway data shows that the normal operating temperature for the battery should be less than 59.5 °C. Based on the model and this temperature, it is found that the maximum safe charge current has a power relationship with the ambient temperature. If the charge current is according with the simulation result, it will be very effective for preventing thermal runaway during battery charging. Besides, the research on relationship of battery geometry and maximum safe charge current will provide a method for both the battery optimization design and the BTMS design.

The significance of this work is to be able to provide the safe value of charging current and the guidance on the safe use of the battery. Also, the scanning results will be favorable to the battery design.

Acknowledgments

We gratefully acknowledge the financial support of National Key Research and Development Program of China (2017YFB0102000, 2017YFB0102003), National Natural Science Foundation of China (21603179,21621091), the Fundamental Research Funds for the Central Universities (20720170021).

Appendix A. Supplementary data

Supplementary data to this article can be found online at https://doi.org/10.1016/j.jpowsour.2019.226971.

Nomenclature

$L_i(\mu m)$	Thickness
ε_s	Solid volume fraction
ε_l	liquid volume fraction
$c_{s,max}$	Maximum theoretical concentration of Li+
c_0	Initial theoretical concentration of Li+
SOC_{max}	Maximum state of charge
SOC_{min}	Minimum state of charge
R_i	Radius distance variable of the solid particles
t_+^0	Li + transference number
ρ_i	Density
D_s	Diffusion coefficient of lithium in the solution phase
b_g	Maximum theoretical loading
α	Charge transfer coefficient
γ	Bruggeman tortuosity factor
λ_i	Thermal conductivity
C_p	Heat capacity
σ_i	Electronic conductivity of solid phase
E_{eq}	Equilibrium potential
R_f	Film resistance
c	Electrolyte concentration
c_{ref}	Reference electrolyte concentration
$\frac{\partial E_{eq}}{\partial T}$	Entropic coefficient
$\frac{\partial lnf}{\partial \ln c}$	Activity coefficient

References

[1] D. Larcher, J.-M. Tarascon, Towards greener and more sustainable batteries for electrical energy storage, Nat. Chem. 7 (2015) 19–29, https://doi.org/10.1038/nchem.2085.

[2] X. Dong, L. Chen, J. Liu, S. Haller, Y. Wang, Y. Xia, Environmentally-friendly aqueous Li (or Na)-ion battery with fast electrode kinetics and super-long life, Sci. Adv. 2 (2016), e1501038, https://doi.org/10.1126/sciadv.1501038.

[3] Y. Gong, Y. Yu, K. Huang, J. Hu, C. Li, Evaluation of lithium-ion batteries through the simultaneous consideration of environmental, economic and electrochemical performance indicators, J. Clean. Prod. 170 (2018) 915–923, https://doi.org/10.1016/j.jclepro.2017.09.189.

[4] M.A. Cusenza, S. Bobba, F. Ardente, M. Cellura, F. Di Persio, Energy and environmental assessment of a traction lithium-ion battery pack for plug-in hybrid electric vehicles, J. Clean. Prod. 215 (2019) 634–649, https://doi.org/10.1016/j.jclepro.2019.01.056.

[5] N. Nitta, F. Wu, J.T. Lee, G. Yushin, Li-ion battery materials: present and future, Mater. Today 18 (2015) 252–264, https://doi.org/10.1016/j.mattod.2014.10.040.

[6] F. Bai, M. Chen, W. Song, Z. Feng, Y. Li, Y. Ding, Thermal management performances of PCM/water cooling-plate using for lithium-ion battery module based on non-uniform internal heat source, Appl. Therm. Eng. 126 (2017) 17–27, https://doi.org/10.1016/j.applthermaleng.2017.07.141.

[7] W. Mei, H. Chen, J. Sun, Q. Wang, The effect of electrode design parameters on battery performance and optimization of electrode thickness based on the electrochemical–thermal coupling model, Sustain. Energy Fuels. 3 (2019) 148–165, https://doi.org/10.1039/C8SE00503F.

[8] X. Feng, S. Zheng, X. He, L. Wang, Y. Wang, D. Ren, M. Ouyang, Time sequence map for interpreting the thermal runaway mechanism of lithium-ion batteries with LiNixCoyMnzO2 cathode, Front. Energy Res. 6 (2018), https://doi.org/10.3389/fenrg.2018.00126.

[9] Y.-S. Duh, K.H. Lin, C.-S. Kao, Experimental investigation and visualization on thermal runaway of hard prismatic lithium-ion batteries used in smart phones, J. Therm. Anal. Calorim. 132 (2018) 1677–1692, https://doi.org/10.1007/s10973-018-7077-2.

[10] M. Ouyang, X. Feng, X. Han, L. Lu, Z. Li, X. He, A dynamic capacity degradation model and its applications considering varying load for a large format Li-ion battery, Appl. Energy 165 (2016) 48–59, https://doi.org/10.1016/j.apenergy.2015.12.063.

[11] Z.P. Cano, D. Banham, S. Ye, A. Hintennach, J. Lu, M. Fowler, Z. Chen, Batteries and fuel cells for emerging electric vehicle markets, Nat. Energy. 3 (2018) 279–289, https://doi.org/10.1038/s41560-018-0108-1.

[12] M. Singer, Consumer Views on Plug-In Electric Vehicles – National Benchmark Report, second ed., 2016, https://doi.org/10.2172/1335806.

[13] J. Liang, F. Li, H.-M. Cheng, High-capacity lithium ion batteries: bridging future and current, Energy Storage Mater. 4 (2016) A1–A2, https://doi.org/10.1016/j.ensm.2016.05.010.

[14] S. Ahmed, S.E. Trask, D.W. Dees, P.A. Nelson, W. Lu, A.R. Dunlop, B.J. Polzin, A. N. Jansen, Cost of automotive lithium-ion batteries operating at high upper cutoff voltages, J. Power Sources 403 (2018) 56–65, https://doi.org/10.1016/j.jpowsour.2018.09.037.

[15] X. Feng, S. Zheng, X. He, L. Wang, Y. Wang, D. Ren, M. Ouyang, Time sequence map for interpreting the thermal runaway mechanism of lithium-ion batteries with LiNixCoyMnzO2 cathode, Front. Energy Res. 6 (2018), https://doi.org/10.3389/fenrg.2018.00126.

[16] X. Zuo, J. Zhu, P. Müller-Buschbaum, Y.-J. Cheng, Silicon based lithium-ion battery anodes: a chronicle perspective review, Nano Energy 31 (2017) 113–143, https://doi.org/10.1016/j.nanoen.2016.11.013.

[17] Z. Liu, Q. Yu, Y. Zhao, R. He, M. Xu, S. Feng, S. Li, L. Zhou, L. Mai, Silicon oxides: a promising family of anode materials for lithium-ion batteries, Chem. Soc. Rev. 48 (2019) 285–309, https://doi.org/10.1039/C8CS00441B.

[18] H. Wu, Y. Cui, Designing nanostructured Si anodes for high energy lithium ion batteries, Nano Today 7 (2012) 414–429, https://doi.org/10.1016/j.nantod.2012.08.004.

[19] R. Hu, W. Sun, Y. Chen, M. Zeng, M. Zhu, Silicon/graphene based nanocomposite anode: large-scale production and stable high capacity for lithium ion batteries, J. Mater. Chem. 2 (2014) 9118–9125, https://doi.org/10.1039/C4TA01013B.

[20] P. Röder, B. Stiaszny, J.C. Ziegler, N. Baba, P. Lagaly, H.-D. Wiemhöfer, The impact of calendar aging on the thermal stability of a LiMn2O4–Li(Ni1/3Mn1/3Co1/3)O2/graphite lithium-ion cell, J. Power Sources 268 (2014) 315–325, https://doi.org/10.1016/j.jpowsour.2014.06.040.

[21] C.K. Chan, R. Ruffo, S.S. Hong, Y. Cui, Surface chemistry and morphology of the solid electrolyte interphase on silicon nanowire lithium-ion battery anodes, J. Power Sources 189 (2009) 1132–1140, https://doi.org/10.1016/j.jpowsour.2009.01.007.

[22] S.C. Jung, H.-J. Kim, J.-H. Kim, Y.-K. Han, Atomic-level understanding toward a high-capacity and high-power silicon oxide (SiO) material, J. Phys. Chem. C 120 (2016) 886–892, https://doi.org/10.1021/acs.jpcc.5b10589.

[23] T. Chen, J. Wu, Q. Zhang, X. Su, Recent advancement of SiOx based anodes for lithium-ion batteries, J. Power Sources 363 (2017) 126–144, https://doi.org/10.1016/j.jpowsour.2017.07.073.

[24] Z. Wang, Y. Fu, Z. Zhang, S. Yuan, K. Amine, V. Battaglia, G. Liu, Application of Stabilized Lithium Metal Powder (SLMP®) in graphite anode – a high efficient prelithiation method for lithium-ion batteries, J. Power Sources 260 (2014) 57–61, https://doi.org/10.1016/j.jpowsour.2014.02.112.

[25] J.R. Szczech, S. Jin, Nanostructured silicon for high capacity lithium battery anodes, Energy Environ. Sci. 4 (2011) 56–72, https://doi.org/10.1039/C0EE00281J.

[26] H.-J. Noh, S. Youn, C.S. Yoon, Y.-K. Sun, Comparison of the structural and electrochemical properties of layered Li[NixCoyMnz]O2 (x = 1/3, 0.5, 0.6, 0.7, 0.8 and 0.85) cathode material for lithium-ion batteries, J. Power Sources 233 (2013) 121–130, https://doi.org/10.1016/j.jpowsour.2013.01.063.
[27] J. Ye, H. Chen, Q. Wang, P. Huang, J. Sun, S. Lo, Thermal behavior and failure mechanism of lithium ion cells during overcharge under adiabatic conditions, Appl. Energy 182 (2016) 464–474, https://doi.org/10.1016/j.apenergy.2016.08.124.
[28] R. Spotnitz, J. Franklin, Abuse behavior of high-power, lithium-ion cells, J. Power Sources 113 (2003) 81–100, https://doi.org/10.1016/S0378-7753(02)00488-3.
[29] X. Feng, M. Ouyang, X. Liu, L. Lu, Y. Xia, X. He, Thermal runaway mechanism of lithium ion battery for electric vehicles: a review, Energy Storage Mater. 10 (2018) 246–267, https://doi.org/10.1016/j.ensm.2017.05.013.
[30] Q. Wang, P. Ping, X. Zhao, G. Chu, J. Sun, C. Chen, Thermal runaway caused fire and explosion of lithium ion battery, J. Power Sources 208 (2012) 210–224, https://doi.org/10.1016/j.jpowsour.2012.02.038.
[31] N.E. Galushkin, N.N. Yazvinskaya, D.N. Galushkin, Mechanism of thermal runaway in lithium-ion cells, J. Electrochem. Soc. 165 (2018), https://doi.org/10.1149/2.0611807jes. A1303–A1308.
[32] J. Yan, Q. Wang, K. Li, J. Sun, Numerical study on the thermal performance of a composite board in battery thermal management system, Appl. Therm. Eng. 106 (2016) 131–140, https://doi.org/10.1016/j.applthermaleng.2016.05.187.
[33] M. Doyle, Comparison of modeling predictions with experimental data from plastic lithium ion cells, J. Electrochem. Soc. 143 (1996) 1890, https://doi.org/10.1149/1.1836921.
[34] L. Cai, R.E. White, Mathematical modeling of a lithium ion battery with thermal effects in COMSOL Inc. Multiphysics (MP) software, J. Power Sources 196 (2011) 5985–5989, https://doi.org/10.1016/j.jpowsour.2011.03.017.
[35] Y. Ye, Y. Shi, N. Cai, J. Lee, X. He, Electro-thermal modeling and experimental validation for lithium ion battery, J. Power Sources 199 (2012) 227–238, https://doi.org/10.1016/j.jpowsour.2011.10.027.
[36] J. Sturm, A. Rheinfeld, I. Zilberman, F.B. Spingler, S. Kosch, F. Frie, A. Jossen, Modeling and simulation of inhomogeneities in a 18650 nickel-rich, silicon-graphite lithium-ion cell during fast charging, J. Power Sources 412 (2019) 204–223, https://doi.org/10.1016/j.jpowsour.2018.11.043.
[37] L. Ai, M. Jia, S. Du, B. Yin, S. Woo, H. Zhang, 3D simulation on the internal distributed properties of lithium-ion battery with planar tabbed configuration, J. Power Sources 293 (2015) 993–1005, https://doi.org/10.1016/j.jpowsour.2015.06.034.
[38] L. Cai, R.E. White, Mathematical modeling of a lithium ion battery with thermal effects in COMSOL Inc. Multiphysics (MP) software, J. Power Sources 196 (2011) 5985–5989, https://doi.org/10.1016/j.jpowsour.2011.03.017.
[39] Y. Ye, Y. Shi, N. Cai, J. Lee, X. He, Electro-thermal modeling and experimental validation for lithium ion battery, J. Power Sources 199 (2012) 227–238, https://doi.org/10.1016/j.jpowsour.2011.10.027.
[40] X. Feng, M. Fang, X. He, M. Ouyang, L. Lu, H. Wang, M. Zhang, Thermal runaway features of large format prismatic lithium ion battery using extended volume accelerating rate calorimetry, J. Power Sources 255 (2014) 294–301, https://doi.org/10.1016/j.jpowsour.2014.01.005.
[41] S.J. An, J. Li, C. Daniel, D. Mohanty, S. Nagpure, D.L. Wood, The state of understanding of the lithium-ion-battery graphite solid electrolyte interphase (SEI) and its relationship to formation cycling, Carbon 105 (2016) 52–76, https://doi.org/10.1016/j.carbon.2016.04.008.